MAGNETOHYDRODYNAMICS Vol. 59 (2023), No. 3-4, pp. 357–363
DOI: 10.22364/mhd.59.3-4.8

INVESTIGATION OF THERMOELECTROMAGNETIC EFFECT AT METAL WIRE ARC ADDITIVE MANUFACTURING

I. Kaldre, V. Felcis*

University of Latvia, 3 Jelgavas str., Riga LV-1004, Latvia
** e-Mail: imants.kaldre@lu.lv*

Metal additive manufacturing (AM) is a rapidly developing new technology. During the AM process, a small quantity of metal is melted and then solidified. During the melting phase, a small melt pool is formed, where different physical phenomena take place which affect the heat and mass transfer in the melt pool and, hence, the solidified material morphology and microstructure. Solid and liquid phases have different Seebeck coefficients, thus, when subjected to a high thermal gradient, thermoelectric currents may appear at the solid-liquid interface. If exposed to the magnetic field, the Lorentz force drives the liquid phase convection. This small-scale melt circulation allows controlling heat and mass transfer. Different direction and strength of the magnetic field allow achieving a different convection type. In this work, we present an experimental scale model to quantify the role of thermoelectromagnetic effect in a melt pool during the wire arc additive manufacturing process. The experimental setup is a copper hemispherical cavity filled with liquid GaInSn with an immersed cobalt electrode. Heat flux is applied through the cobalt electrode, and thermoelectric currents are generated at the interface between the electrode and the liquid metal. The liquid metal motion created by different orientations of the static magnetic field up to 0.1 T is measured. This result is compared with the numerical model and analytical estimations. Experimental and numerical results demonstrate that the thermoelectromagnetic effect can be significant during the additive manufacturing process.

Introduction. Metal additive manufacturing using an electric arc is one of the most popular wire-fed additive manufacturing methods. This method is cheaper and faster but less accurate than the laser metal additive manufacturing. During this process, a small melt pool of liquid metal is created by melting the supplied wire by an electric arc. The heat and mass transfer in this melt pool determines the microstructure formation and properties of the solidified material [1]. These properties are mainly determined by the cooling rate of the melted and heated metal.

One of the prospective approaches is the application of an external magnetic field, which can significantly affect the melt pool flow and consequently affect the solidified structure and properties [2]. The magnetic field has several different effects on the liquid metal flow. Particularly interesting is the thermoelectromagnetic effect. It is important to understand how it can affect the actual additive manufacturing process. The thermoelectric current is induced between the electrode and the liquid metal if the interface is subjected to a temperature gradient [3]. Cobalt is chosen as an electrode material in this study because of its high Seebeck coefficient and relatively good electrical conductivity. It is known that the thermoelectric effect combined with an external magnetic field can drive convection of the liquid phase. Thermoelectromagnetic convection (TEMC) can be the dominant flow in certain cases because this convection can be generated at a very small length scale comparable with the viscous boundary layer. This phenomenon is observed during the dendritic solidification of metallic alloys, where a large local thermal gradient is present [4-6]. Depending on the magnetic field direction, convection patterns can be very different. It is shown that in an axial magnetic field with primary dendrite arms, the fluid rotates around the dendrite arm. If the magnetic field is transverse, a

crucible-scale convection is driven perpendicularly to the direction of the magnetic field and a crucible size segregation is observed [7].

It is difficult to investigate this process directly because of the small scale, rapid process, and high temperature, thus we have developed a large-scale model, where we can have a look at different physical phenomena occurring in the liquid metal pool and later use the results for better understanding of the AM processes. Such experimental setup can be used to measure actual liquid metal velocities by applying Ultrasound Doppler Velocimetry (UDV) or tracer particles at the surface [8]. A similar laboratory experiment has been developed to investigate electrovortex flow in liquid metal under combined AC magnetic fields [9].

1. Experimental.

The experimental setup used in this study is a hemispherical copper cavity ($R = 30$ mm) filled with a liquid GaInSn alloy; a cobalt electrode ($r = 5$ mm) is immersed in the liquid metal pool (Fig. 1*a*). An external magnetic field ($B = 0.1$ T) is generated by a permanent magnet system which is placed around the central part of the experimental setup. A heat flux is created by a 200 W electric heater around the top of the cobalt electrode. The outer part of the copper electrode is kept at room temperature. In this situation, the heat flux through the cobalt electrode creates a thermal gradient along the electrode interface with GaInSn and a thermoelectric current circulates at the interface. The experimental setup is displayed in Fig. 1*b*.

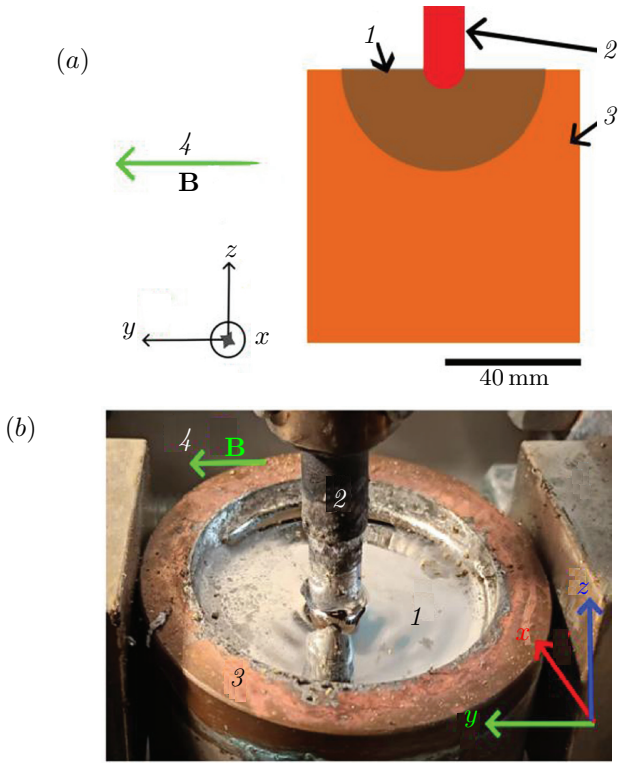

Fig. 1. (*a*) Schematic view of the experimental setup. (*b*) Experimental setup photo; *1* – liquid GaInSn, *2* – cobalt electrode, *3* – copper hemisphere, *4* – magnetic field.

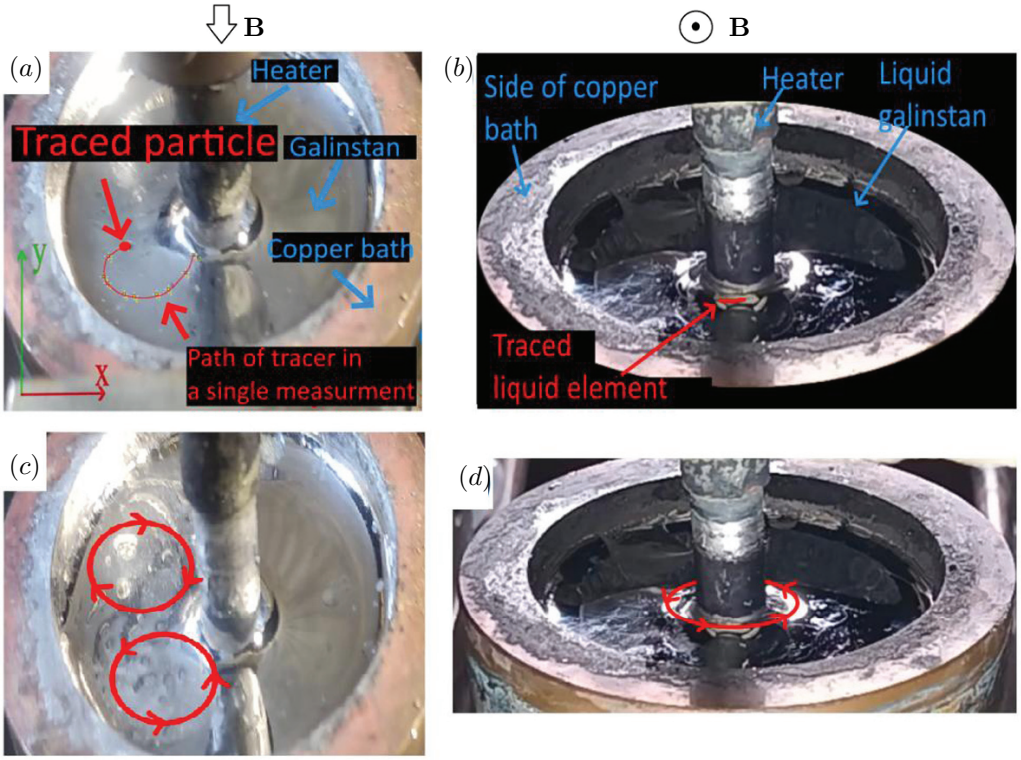

Fig. 2. TEMC in the liquid metal pool. (*a*), (*c*) Path of the traced particle, transverse MF $B = 0.1$ T; (*b*),(*d*) liquid metal free surface coated with HCl solution, axial MF $B = 0.1$ T.

In this study, we made velocity measurements by observing the metal free surface or tracer particles on the surface. To examine the liquid metal flow before observation, the surface was treated with a hydrochloric acid solution to reduce the oxidation. Figs. 2*a*,*c* show the analysis of the experiment with a transverse DC magnetic field, whereas Figs. 2*b*,*d* show the axial magnetic field case. In general, the observed flow agrees well with previously predicted flow characteristics. Under the transverse magnetic field the flow perpendicular to the magnetic field is driven while with the axial magnetic field rotation around the central electrode takes place.

2. Analytical description.

The experimental setup is designed to maximize the thermoelectromagnetic effect and to ensure the opportunity to make direct experimental measurements of the liquid GaInSn convection driven by the thermoelectric current and magnetic field. Different physical phenomena appeared in this experiment. For analytical description of the process, we used a stationary, incompressible fluid model. Heat was transferred by conduction in solid parts, while in the liquid phase the convective heat transfer is also considered according to equation

$$\rho c \mathbf{u} \cdot \nabla T + \nabla \cdot (-k \nabla T) = q, \tag{1}$$

where ρ is the density, c is the thermal capacity, q is the volumetric heat source, k is the thermal conductivity, μ is the dynamic viscosity, γ is the surface tension, L is the characteristic length scale.

The current flow in continuous media is described by the Ohm's law,

$$\mathbf{j} = \sigma\left(\mathbf{E} + \mathbf{u} \times \mathbf{B} - \mathrm{S}\nabla T\right), \tag{2}$$

S is the Seebeck coefficient.

The generation of thermoelectric potential at the interface between the liquid GaInSn and the solid cobalt electrode can be described by the boundary condition given by Shercliff [3]:

$$\frac{j_{1\mathrm{t}}}{\sigma_1} - \frac{j_{2\mathrm{t}}}{\sigma_2} + u_{\mathrm{s}} B_{\mathrm{n}} = \Delta\mathrm{S}\frac{\mathrm{d}T}{\mathrm{d}t}, \tag{3}$$

where 'n' and 't' denote the normal and tangential components, while 's' denotes the out of plane tangential component, indices 1 and 2 denote the properties of cobalt and GaInSn. The fluid flow is governed by the stationary Navier-Stokes equation which balances all volume force densities acting on the fluid element:

$$\rho\mathbf{u} \cdot \nabla\mathbf{u} = -\nabla p + \mu\nabla^2\mathbf{u} + \sigma\mathbf{u} \times \mathbf{B} \times \mathbf{B} + \sigma\mathrm{S}\nabla T \times \mathbf{B}, \tag{4}$$

dimensionless numbers characterizing the ratios between different effects are calculated to understand the significance of the effects which are considered in the numerical model and in the interpretation of the experiments. A Marangoni force appears on the free surface of the liquid GaInSn when subjected to a temperature gradient. The Marangoni stress on the surface can be expressed as $f = \partial\gamma/\partial r$, [N/m^2].

A force appears due to the temperature variation along the electrode, causing the liquid metal to ascend near the electrode . The material properties used in the calculations and numerical models are summarized in Table 1.

The ratio between viscous and inertial forces is characterized by the Reynolds number $\mathrm{Re} = \rho u L/\mu$. The ratio between conductive and convective heat transfer is the Peclet number $\mathrm{Pe}_L = L\rho c u/k$. The Grasshoff number $\mathrm{Gr} = L^3\rho_2\beta\Delta T g/\mu^2$ characterizes the ratio between buoyancy and viscous forces. The Marangoni number $\mathrm{Ma} = (\mathrm{d}\gamma/\mathrm{d}r)(L\rho c\Delta T/(\mu k))$ determines the ratio between the Marangoni force and viscous force. The magnetic field induced by the motion of the liquid metal is characterized by the Stuart number $\mathrm{N} = B^2 L\sigma/(\rho u)$. In this calculation, we assume the characteristic length $L = 1$ cm, the characteristic velocity can be estimated by balancing the thermoelectric term and the inertial term in the Navier–Stokes equation:

$$u = \sqrt{\frac{L\sigma B\mathrm{S}\nabla T}{\rho}}. \tag{5}$$

Table 1. Physical properties of the materials.

Property/material	Symbol	GaInSn	Cobalt	Copper
Density (at 20°C)	ρ_0 [kg/m^3]	6360	8900	8940
Thermal conductivity	k [W/(m·K)]	16	100	398
Heat capacity	c [J/kg·K]	371	450	386
Electric conductivity	σ [MS/m]	3.3	16	58
Seebeck coefficient	S [μV/K]	–0.4	–25	2
Dynamic viscosity	μ [Pa·s]	0.03		
Volumetric thermal expansion	β [1/m^3]	$1.22{\cdot}10^{-4}$		
Surface tension	γ [N/m]	$0.58–1.09{\cdot}10^{-5}T$ [K]		

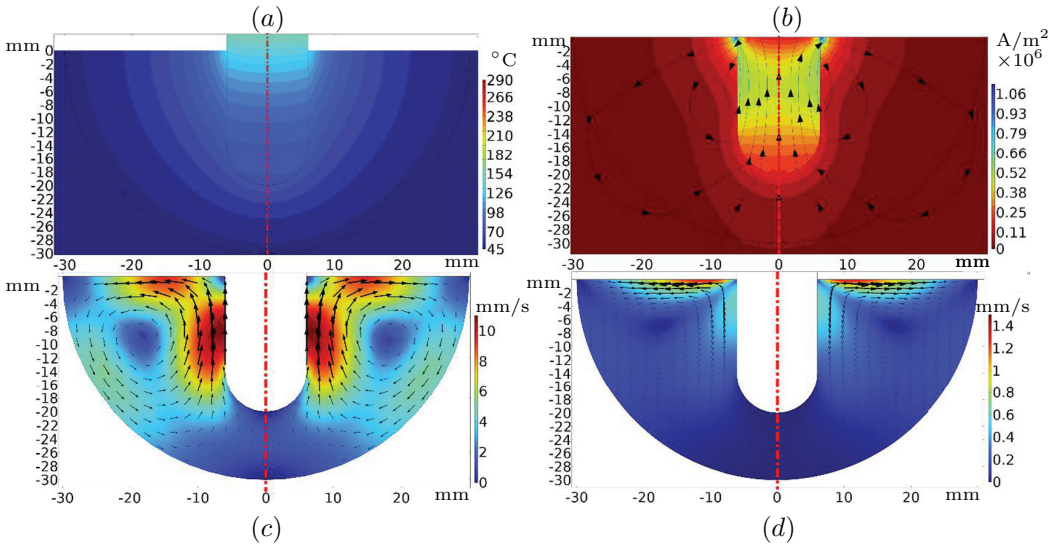

Fig. 3. Numerical simulation results: (*a*) temperature distribution; (*b*) thermoelectric current distribution; (*c*) buoyancy velocity; (*d*) Marangoni velocity.

The estimation from Eq. (5) gives the characteristic TEMC velocity of $u = 34$ cm/s.

The calculation of the dimensionless numbers gives $\mathrm{Re} = 150$, $\mathrm{Pe} = 100$, $\mathrm{Gr} = 2700$, $\mathrm{Ma} = 30$, $\mathrm{N} = 2$. This means that we can use the laminar flow approximation where the convective heat transfer is important and the electromagnetic force is comparable with inertial forces. The aim of this experiment was to investigate the role and the possible magnitude of the thermoelectromagnetic effect, so we did not analyze the role of the electric arc and the weld current interaction with the magnetic field and its impact on the overall process.

In the experiment, we primarily optically observed the free surface to examine the velocity field on the liquid metal pool surface. Tracer particles on the surface were tracked and the velocity of the liquid metal was measured. The measured velocity magnitude is up to 10–15 cm/s, however, accurate mapping of the velocity field was complicated. The liquid metal free surface oxidation is one of the problems limiting our ability to observe the flow pattern in the liquid metal from the surface. A weak HCl acid solution was used to dissolve this oxide film for better observations.

3. Numerical model.

Different physical phenomena were calculated using the Comsol 6.0 software. Thermal, electromagnetism and 3D fluid flow in the laminar approximation was calculated. The numerically calculated temperature and temperature gradient is shown in Fig. 3*a*. The calculated thermoelectric current distribution is shown in Fig. 3*b*.

The velocity of thermoelectromagnetic convection under the axial magnetic field is shown in Figs. 4*a*,*b*, and under the transverse magnetic field in Figs. 4*c*,*d*. The results show that the localized liquid metal velocities are up to 20 cm/s. These results are in good agreement with the estimation of the TEMC velocity and flow morphology predicted before and with the results published in previous works investigating the TEMC distribution around a free particle [10].

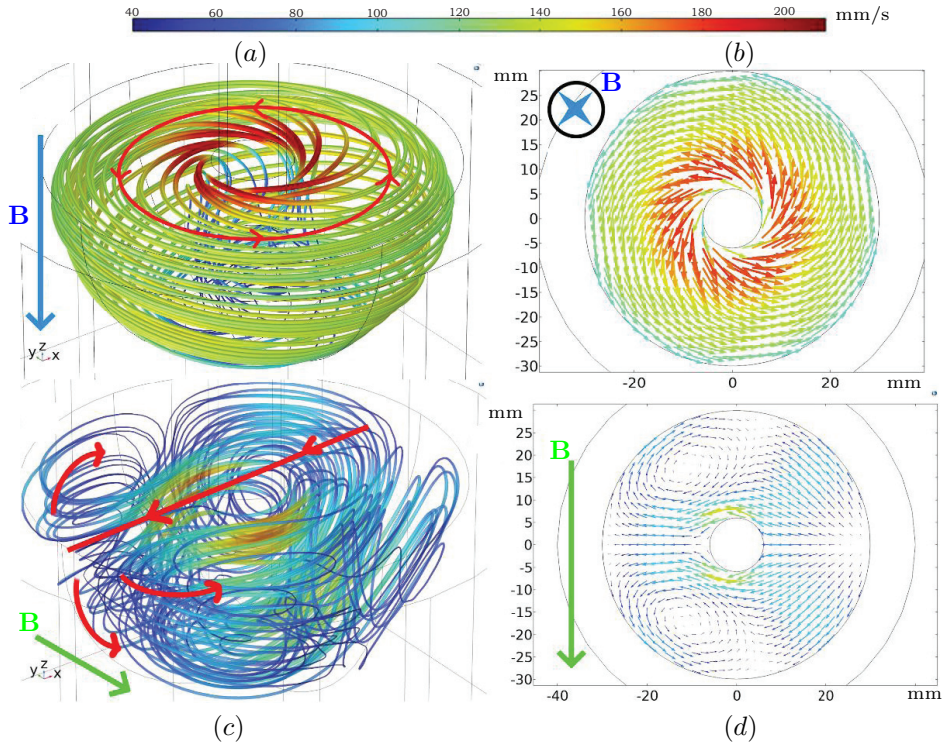

Fig. 4. (*a*), (*b*) TEMC velocity under the axial magnetic field $B = 0.1$ T; (*c*), (*d*) TEMC velocity under the transverse magnetic field $B = 0.1$ T.

The calculated buoyancy velocity is shown in Fig. 3*c* and the Marangoni velocity in Fig. 3*d*. The flow velocity due to buoyancy (Fig. 3*c*) and Marangoni (Fig. 3*d*) effects is much smaller than the thermoelectromagnetic flow velocity, so these effects do not significantly influence the resulting flow field.

4. Conclusions.

In this paper, it was shown that the thermoelectromagnetic force can initiate a significant liquid phase flow. In an actual additive manufacturing situation, a large thermal gradient is present, thus TEMC can be the source of a strong molten metal flow. One of the methods to influence the liquid metal flow in the melt pool during additive manufacturing is to use a magnetic field and, therefore, to influence also the solidified structure of the metal. The agreement between the observed and numerically calculated results and the analytical prediction of the behavior of the melt pool under an external DC magnetic field was found to be good. The predicted and the observed liquid metal motion agree well; also a good agreement was found between the order of magnitude of velocity estimation and observation and the numerical model. This study can be used to estimate the significance of these effects in the actual additive manufacturing situation.

References

[1] C. Liu, H. Gao, L. Li *et al.* A review on metal additive manufacturing: modeling and application of numerical simulation for heat and mass transfer and microstructure evolution. *China Foundry*, vol. 18(2021), pp. 317–334.

[2] A. Kao, T. Gan, C. Tonry, I. Krastins, K. Pericleous. Thermoelectric magnetohydrodynamic control of melt pool dynamics and microstructure evolution in additive manufacturing. *Phil. Trans. R. Soc. A*, vol. 378 (2020): 20190249.

[3] J. Shercliff. Thermoelectric magnetohydrodynamics. *J. Fluid Mechanics*, vol. 91 (1979), no. 2, pp. 231–251.

[4] I. Kaldre, Y. Fautrelle, J. Etay, A. Bojarevics, L. Buligins. Thermoelectric current and magnetic field interaction influence on the structure of directionally solidified Sn10 wt.%Pb alloy. *J. Alloys and Compounds*, vol. 571(2013), pp. 50–55.

[5] L. Xi, A. Gagnoud, Z. Ren, Y. Fautrelle, R. Moreau. Investigation of thermoelectric magnetic convection and its effect on solidification structure during directional solidification under a low axial magnetic field. *Acta Materialia*, vol. 57 (2009), no. 7, pp. 2180–2197.

[6] I. Kaldre, Y. Fautrelle, J. Etay, A. Bojarevics, L. Buligins. Investigation of liquid phase motion generated by the thermoelectric current and magnetic field interaction. *Magnetohydrodynamics*, vol. 46 (2010), no. 4, pp. 371–380.

[7] I. Kaldre, A. Bojarevics, Y. Fautrelle, J. Etay, L. Buligins. Current and magnetic field interaction influence on liquid phase convection. *Magnetohydrodynamics*, vol. 48 (2012), no. 2, pp. 399–406.

[8] I. Kaldre, C. Wang, R. Baranovskis. Experimental investigation of weld pool flow under external DC magnetic field. *Magnetohydrodynamics*, vol. 55 (2019), no. 4, pp. 469–474.

[9] D.A. Vinogradov, I.O. Teplyakov, Yu.P. Ivochkin, A. Kharicha. On the applicability of the electrodynamic approximation in the simulation of the electrovortex flow in the presence of an external magnetic field. *IOP Conf. Series: J. Physics: Conf. Series*, vol. 101 1128 (2018), 012112.

[10] J. Wang, Y. Fautrelle, Z. Ren *et al.* Thermoelectric magnetic force acting on the solid during directional solidification under a static magnetic field. *Appl. Phys. Lett.*, vol. 101 (2012), 251904.

Received 22.12.2023